Journal of Electroceramics 3:3, 301–310, 1999

Influence of Water Vapor on the Response of Mg-Doped $SrTiO_3$ Ceramic Oxygen Sensors

HONG ZHENG & O. TOFT SØRENSEN*
Materials Research Department, Risø National Laboratory, P.O. Box 49, DK-4000, Roskilde, Denmark

LIU XINGQIN
Department of Materials Science and Engineering, University of Sci. & Tech. of China, 230026, Hefei, Anhui, P.R. of China

HENNING JENSEN
PBI-Dansensor A/S, Rønnedevej 18, DK-4100, Ringsted, Denmark

Submitted November 18, 1998; 1st Revised June 4, 1998; 2nd Revised October 2, 1998; Accepted November 24, 1998

Abstract. Mg-doped $SrTiO_3$ thick film sensors fabricated by screen-printing proved to be very promising for the use as oxygen sensors. A study of the influence of water on the response of these sensors gives an important basis for understanding their behavior in practical applications. The influence of water on the sensor response was measured in the oxygen partial pressure region from air (0.21 bar) to pure N_2 (2.5×10^{-5} bar) and the temperature range from 600 to 800°C. The relative humidity was varied from 1 to 95% RH. The resistance variation as a function of temperature and the activation energy were evaluated under different dry and wet conditions. The results obtained show that the resistance of these sensors generally decreases with increasing water content in the carrier gas and that the effect of water was strongest at lower temperatures as well as at lower oxygen pressures. To explain this behavior, it is proposed that a partial proton conduction is introduced in the water-containing atmospheres and that this contributes to the total conductivity leading to a reduction of the total resistance. Finally, the measurements also show that the response of these sensors still depends on the oxygen partial pressure according to the standard expression even in the presence of water vapor. Therefore, these sensors can still be used as oxygen sensors in humid atmospheres.

Keywords: oxygen sensor, defect chemistry, Mg-doped $SrTiO_3$ ceramic, water influence, proton conduction

1. Introduction

Due to the strict legislation for emission control of motor vehicles, the need of modern cost-effective and reliable oxygen sensors for controlling the air-to-fuel ratio (A/F) of the exhaust gas is becoming increasingly important [1]. At present, the electrochemical ZrO_2 sensors are widely used for this purpose, but recently, semiconducting-type oxygen sensors have become more promising for this application due to their small sizes, simple structures and low costs.

*Author to whom correspondence should be addressed: O. Toft Sørensen, Fax: (+45) 46775758, Tel: (+45) 46775716, E-mail: o.toft.sorensen@risoe.dk

The semiconducting oxygen sensor is based on its changes in resistance according to the oxygen partial pressure of the surrounding atmosphere. Of all the metal oxides sensitive to the presence of oxygen in this manner, $SrTiO_3$ has been selected as one of the most promising materials [2]. Normally, this compound exhibits *p*-type conduction at high oxygen partial pressures, and *n*-type conduction at low oxygen partial pressures. In practice, it is however very important that this *p-n* transition should not occur in the oxygen partial pressure region where the sensor is applied. It is suggested that partial substitution of Mg^{2+} for Ti^{4+} in $SrTiO_3$ shifts the *p-n* transition to lower oxygen partial pressures [3], giving an

improvement of the oxygen-sensing properties of Mg-doped $SrTiO_3$ in the *p*-type region as well. As reported in our previous work [4], the sensor based on Mg-doped $SrTiO_3$ exhibits a high oxygen sensitivity in N_2/O_2 mixtures in the P_{O_2} region from 10^{-1} to 10^{-5} atm.

However, under practical field conditions, the gas atmospheres often contain water vapor and other, in some cases, very reactive components in addition to oxygen and nitrogen. Considering the possible chemical reactions, these gaseous components may change the oxygen partial pressure in the atmosphere, which can generate or annihilate oxygen vacancies in the metal oxide [5]. The presence of these gases therefore has a direct effect on the electrical behavior of the sensors. This makes it necessary to investigate the possible interference of different atmospheres on the response of the sensors.

As stressed by several authors, these gas sensors are specially sensitive to humidity [6], which has been considered as one of the main interferences to sensor response.

In the present work, the effect of humidity on the sensor response was examined and a model based on defect structures and conduction mechanisms of this oxide is proposed to describe the experimental results.

2. Theory

2.1. Defect Chemistry and Resistance Dependence on Oxygen Partial Pressure of Mg-doped $SrTiO_3$ in Dry Atmospheres

The details of the defect chemistry of Mg-doped $SrTiO_3$ in dry atmospheres have been discussed in [7]. It is suggested that the incorporation of Mg^{2+} in $SrTiO_3$ on the Ti site results in the formation of oxygen vacancies. Normally, this oxide exhibits *p*-type conduction in the high oxygen partial pressure region ($P_{O_2} > 10^{-6}$ atm). Electron holes are formed by a reaction between oxygen in the surrounding atmosphere and these oxygen vacancies:

$$\frac{1}{2}O_2 + V_O^{\bullet\bullet} \leftrightarrow O_O^{\times} + 2h^{\bullet} \tag{1}$$

As reported in our previous work [8], the electrical conductivity of Mg-doped $SrTiO_3$ in this *p*-type region can therefore be expressed as:

$$\sigma_p = K_1(T)^{1/2}[Mg''_{Ti}]^{1/2} e\mu_p P_{O_2}^{1/4} \tag{2}$$

where e is the electronic charge, μ_P, the hole mobility and $K_1(T)$ is the equilibrium constant for reaction (1).

It has been reported [9] that the hole mobility of *p*-type conducting $SrTiO_3$ may be described by $\mu_p(T) = 1.1 \times 10^6\,\mathrm{cm}^2(Vs)^{-1}(T/K)^{-2.36}$ in the temperature range of 500° to 1000°C. In this work, using similar mathematical treatment as in [9] for electron mobility, the temperature-dependent hole mobility can be approximated by an exponential law according to:

$$\mu_p(T) = \mu_p^o \exp\left(\frac{E_{\mu_p}}{kT}\right) \tag{3}$$

where μ_p^o is a constant, k is the Boltzmann constant and E_{μ_p} is the thermal activation energy for hole mobility.

The equilibrium constant $K_1(T)$ can be expressed as:

$$K_1(T) = K_1^o \exp(-\Delta H_1/kT) \tag{4}$$

where K_1^o represents a constant and ΔH_1 the enthalpy for reaction (1). A combination of Eqs. (2), (3) and (4) gives a thermally activated electronic hole conductivity expressed by:

$$\sigma = A_1 \exp(-E_p/kT) P_{O_2}^{1/4} \tag{5}$$

where E_p is the thermal activation energy for hole conduction.

According to the relationship between the resistance, R, and the conductivity, σ, $R \propto 1/\sigma$, the resistance R can be thus expressed as:

$$R = B_1 \exp(E_p/kT) P_{O_2}^{-1/4} \tag{6}$$

where B_1 is a constant.

A plot of log R vs. log P_{O_2} should therefore result in a straight line with a slope $(-1/m)$ of $-\frac{1}{4}$ at constant temperatures.

2.2. Thermal Activation Energy for Hole Conduction in Dry Atmospheres

If the oxygen partial pressure is constant, Eq. (6) can be simplified to:

$$R = B_2 \exp(E_p/kT) \tag{7}$$

where B_2 is a constant.

The thermal activation energy E_p can therefore be determined from the slope (n_1) of the Arrhenius plot ($\log R$ vs. $1000/T$) as:

$$\log R = b_1 + n_1(1000/T)$$

with

$$n_1 = E_p/1000k(\ln 10) \text{ and } b_1 = \log B_2 \tag{8}$$

2.3. *Defect Chemistry of Mg-doped $SrTiO_3$ in Wet Atmospheres*

When water vapor is introduced into the surrounding atmosphere, it is assumed [10] that the perovskite-type oxides may dissolve a significant concentration of protons and become partially proton conducting. Water is incorporated into the surface or the bulk of these oxides, annihilating the oxygen vacancies while the protons are attached to the oxygen ions. Once these protonic defects are formed, they may migrate in the lattice [11]. This model can be described by the following three reactions [12]:

(a) Hydrogen enters the lattice by a reaction in which an oxygen ion from water combines with an oxygen vacancy leaving two interstitial protons $(H_i^{\bullet})$, according to:

$$H_2O(g) + V_O^{\bullet\bullet} \rightarrow O_O^{\times} + 2H_i^{\bullet} \tag{9}$$

(b) Hydrogen resides in the lattice as OH^- ions $(OH_O^{\bullet})$ rather than as interstitial protons $H_i^{\bullet}$, which can be expressed by the reaction:

$$H_2O(g) + V_O^{\bullet\bullet} + O_O^{\times} \rightarrow 2OH_O^{\bullet} \tag{10}$$

It has become customary to regard $OH_O^{\bullet}$ as identical to $H_i^{\bullet}$ and the reactions in the form of Eqs. (9) and (10) are therefore equivalent.

(c) Protons migrate by hopping from one O^{2-} ion to another in nearest-neighbor positions in the lattice, as symbolized by:

$$OH \bullet\bullet\bullet O \rightarrow O \bullet\bullet\bullet HO$$

The equilibrium constant $K_2(T)$ of reaction (9) is

$$K_2(T) = [H_i^{\bullet}]^2/[V_O^{\bullet\bullet}]\, P_{H_2O} \tag{11}$$

where $[H_i^{\bullet}]$ and $[V_O^{\bullet\bullet}]$ are the concentrations of protons and oxygen vacancies respectively and P_{H_2O} is the partial pressure of water vapor.

It is interesting to note that this equation implies that the higher the oxygen vacancy concentration, the higher is the concentration of protons. The oxygen vacancies generated by Mg-doping therefore play an important role in the formation of protons in this material [13].

In the case of an atmosphere containing water vapor, the electroneutrality condition will be:

$$2[Mg_{Ti}''] = 2[V_O^{\bullet\bullet}] + [H_i^{\bullet}] + p \tag{12}$$

If it is assumed that $[V_O^{\bullet\bullet}] \gg [H_i^{\bullet}]$, p then the approximation is still [14]:

$$[Mg_{Ti}''] \approx [V_O^{\bullet\bullet}] = \text{constant} \tag{13}$$

The proton concentration $[H_i^{\bullet}]$ at a given P_{H_2O} can thus be derived as:

$$[H_i^{\bullet}] = K_2(T)^{1/2}[Mg_{Ti}'']^{1/2}P_{H_2O}^{1/2} \tag{14}$$

and therefore,

$$\sigma_{H_i^{\bullet}} = e\mu_{H_i^{\bullet}}K_2(T)^{1/2}[Mg_{Ti}'']^{1/2}P_{H_2O}^{1/2} \tag{15}$$

Assuming that the temperature-dependent proton mobility $\mu_{H_i^{\bullet}}$ also follows an exponential law:

$$\mu_{H_i^{\bullet}} = \mu_{H_i^{\bullet}}^{O} \exp\left(\frac{E_{\mu_{H_i^{\bullet}}}}{kT}\right) \tag{16}$$

where $\mu_{H_i^{\bullet}}^{O}$ is a constant and $E_{\mu_{H_i^{\bullet}}}$ is the thermal activation energy for proton mobility.

The equilibrium constant $K_2(T)$ can be expressed as:

$$K_2(T) = K_2^o \exp(-\Delta H_2/kT) \tag{17}$$

where K_2^o represents a constant and ΔH_2 the enthalpy for reaction (9). Combining Eqs. (15), (16) and (17) leads to a thermally activated proton conductivity given by:

$$\sigma_{H_i^{\bullet}} = A_2 \exp(-E_{H_i^{\bullet}}/kT)P_{H_2O}^{1/2} \tag{18}$$

As the contribution of oxygen vacancies ions and electrons to the total conduction is negligible at high and intermediate PO_2 as considered here, the total conductivity may be regarded as the sum of proton and hole conductivity:

$$\begin{aligned}\sigma_{\text{total}} &= \sigma_p + \sigma_{H_i^{\bullet}} \\ &= A_1 \exp(-E_p/kT)P_{O_2}^{1/4} \\ &\quad + A_2 \exp(-E_{H_i^{\bullet}}/kT)P_{H_2O}^{1/2}\end{aligned} \tag{19}$$

2.4. Dependence of Resistance on Oxygen Partial Pressure in Wet Atmospheres

Equation (19) at constant temperature becomes,

$$\sigma_{\text{total}} = \sigma_p^O P_{O_2}^{1/4} + \sigma_{H_i^\bullet}^O P_{H_2O}^{1/2} \tag{20}$$

In this case, the slope $(-1/m)$ of a plot ($\log R$ vs. $\log P_{O_2}$) can be derived as:

$$\begin{aligned}\frac{1}{m} &= -\frac{d(\log R_{\text{total}})}{d(\log P_{O_2})} = \frac{d(\log \sigma_{\text{total}})}{d(\log P_{O_2})} \\ &= \frac{d\log(\sigma_p^O P_{O_2}^{1/4} + \sigma_{H_i^\bullet}^O P_{H_2O}^{1/2})}{d(\log P_{O_2})} \\ &= \frac{1}{4} \times \frac{\sigma_p^O P_{O_2}^{1/4}}{\sigma_p^O P_{O_2}^{1/4} + \sigma_{H_i^\bullet}^O P_{H_2O}^{1/2}} < \frac{1}{4}\end{aligned} \tag{21}$$

This expression demonstrates clearly, that in wet atmospheres, the value of $1/m$ will deviate from the theoretical value $(\frac{1}{4})$ and that it decreases with increasing water partial pressure.

2.5. Thermal Activation Energy for Proton Conduction

Applying Eq. (19), the following equation can be obtained:

$$\begin{aligned}1/R_{\text{total}} \propto (&A_1 \exp(-E_p/kT) P_{O_2}^{1/4} \\ &+ A_2 \exp(-E_{H_i^\bullet}/kT) P_{H_2O}^{1/2})\end{aligned} \tag{22}$$

which in dry conditions becomes:

$$1/R_1 = \left\{A_1 \exp(-E_p/kT) P_{O_2}^{1/4}\right\} \tag{23}$$

and in wet conditions,

$$\begin{aligned}1/R_2 = \Big\{&A_1 \exp(-E_p/kT) P_{O_2}^{1/4} \\ &+ A_2 \exp(-E_{H_i^\bullet}/kT) P_{H_2O}^{1/2}\Big\}\end{aligned} \tag{24}$$

Subtracting Eq. (23) from Eq. (24) gives:

$$(1/R_2 - 1/R_1) = \left\{A_2 \exp(-\mathrm{E}_{\mathrm{H_i^\bullet}}/\mathrm{kT}) \mathrm{P}_{\mathrm{H_2O}}^{1/2}\right\} \tag{25}$$

Thus, plotting the data in the form of $\log(1/R_2 - 1/R_1)$ vs. $1000/T$ at constant water partial pressure, a straight line should be obtained as:

$$\log(1/R_2 - 1/R_1) = b_2 + n_2(1000/T)$$

with

$$n_2 = -E_{H_i^\bullet}/1000k(\ln 10) \text{ and } b_2 = \log(A_2 P_{H_2O}^{1/2}) \tag{26}$$

where $E_{H_i^\bullet}$ is the thermal activation energy for proton conduction.

The thermal activation energy $E_{H_i^\bullet}$ can be therefore calculated from the slope (n_2) of the Arrhenius plot $(\log(1/R_2 - 1/R_1)$ vs. $1000/T)$.

2.7. Proton Transport Number

Finally, the proton transport number $t_{H_i^\bullet}$ can be expressed by:

$$\begin{aligned}t_{H_i^\bullet} &= \frac{\sigma_{H_i^\bullet}}{\sigma_{\text{total}}} \\ &= A_2 \exp(-E_{H_i^\bullet}/kT) P_{H_2O}^{1/2} / \\ &\left\{A_1 \exp(-E_p/kT) P_{O_2}^{1/4} + A_2 \exp(-E_{H_i^\bullet}/kT) P_{H_2O}^{1/2}\right\} \\ &= 1 \Big/ \left\{1 + \frac{A_1}{A_2} P_{O_2}^{1/4} P_{H_2O}^{-1/2} \exp(E_{H_i^\bullet} - E_p)/kT\right\}\end{aligned} \tag{27}$$

3. Experimental

3.1. Synthesis of the Mg-doped $SrTiO_3$ Powder

A flow chart for the preparation of the Mg-doped strontium titanate powder is shown in Fig. 1.

Tetraisopropyl titanate, which was used as the starting material, was mixed with acetic acid and agitated to form a titanyl acylate precursor, which became a clear solution by addition of distilled water. This clear solution was then slowly added to a strong NaOH solution, to which a nitrate solution with the proper Mg^{2+}/Sr^{2+} ratio was also added. The ratio of strontium to titanium was kept at 1:1. The weight ratio of water to titanium alkoxide and the mole ratio of acetic acid to titanium alkoxide were higher than ten in this precursor solution. This precipitation was kept at a temperature of 80°C and it proceeded for 2–3 h to form a white precipitate. The precipitate obtained was washed with water several times to expel any sodium

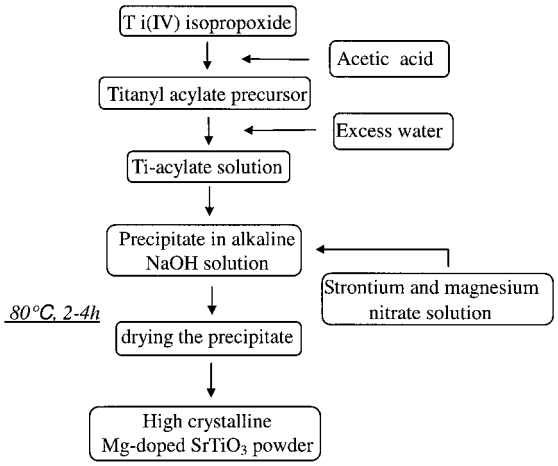

Fig. 1. Low-temperature synthesis route for preparation of Mg-doped $SrTiO_3$ powders.

ions and then dried at 50°C for 20 h. The dried powder was examined by X-ray diffraction (XRD). It was confirmed that the powder was highly crystalline Mg-doped $SrTiO_3$ with the dominating perovskite structure, as shown in Fig. 2. Some small traces of another phase were also observed in the X-ray diffraction pattern, but the presence of this phase was not considered important in the interpretation of the results obtained in this work.

3.2. Sensor Fabrication

The screen-printing technique was used to manufacture the sensors. In this process, a paste is pressed through a screen onto the substrate using a rubber blade. The paste of sensor material suitable for screen-printing was prepared by mixing 55% weight percent of Mg-doped $SrTiO_3$ powder with 45% weight percent of organic binder, which was used to provide the necessary viscosity for the screen-printing process. This paste was ball-milled for 12 h before printing. A commercial platinum paste was used for the fabrication of the electrode films. The platinum electrodes were designed in the form of a rectangular pattern with an average interspacing of 500 μm as shown in Fig. 3.

The Mg-doped $SrTiO_3$ paste was first printed on the whole area of an Al_2O_3 substrate and fired at a maximum temperature of 1200°C for 2 h. The platinum paste was subsequently printed and fired at 1000°C for 2 h on top of this film. Sensors of required size, each containing one or several basic units, were then obtained by laser cutting. Platinum wires, serving as the leads, were then fixed with platinum paste on each individual sensor and the sensors were finally heat treated once more to 900°C for 1 h. After printing and sintering, the platinum electrode film had a thickness of about 10 μm and the Mg-doped $SrTiO_3$ film had a thickness of about 80 μm.

3.3. Measurement Setup

The measurement setup is schematically illustrated in Fig. 3.

In order to determine the dependence of resistance of the Mg-doped $SrTiO_3$ sensors on temperature and P_{O_2}, the sample was placed in a tube furnace, in which the temperature of the sample could be changed by adjusting the voltage of the furnace heater. The actual sample temperature was measured with a thermocouple, which was positioned alongside the sample.

Different oxygen partial pressures were obtained

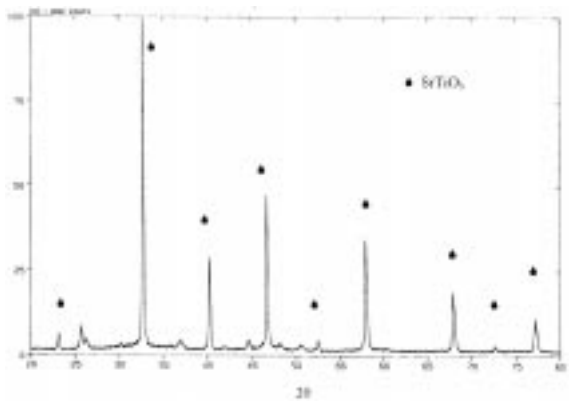

Fig. 2. X-ray diffraction pattern of an as-dried Mg-doped $SrTiO_3$ powder.

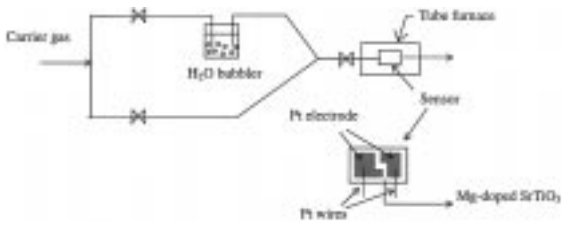

Fig. 3. Schematic illustration of measurement setup and structure of sensor element.

using N_2/air mixtures $(2.5 \times 10^{-5}\,\text{bar} < P_{O_2} < 0.21\,\text{bar})$.

Carrier gases with different water contents were prepared by mixing a dry gas and a humidified gas, which was obtained by the means of passing the gas through a H_2O bubbler at 25°C. Controlling the ratio of these two gases, different humidities could be obtained from 1% to 95% relative humidity. The gas flow past the sample was controlled by a flowmeter, which was set at a constant rate of 100 cc/min.

4. Results

4.1. Resistance as a Function of Temperature Under Different P_{O_2} and Humidity Conditions

In order to evaluate the resistance of the sensor as a function of temperature under the conditions of different P_{O_2} and moisture, measurements were carried out in dry and wet air, 1%O_2/N_2 gas, and N_2 gas respectively. The temperature was varied between 500 and 800°C. Figure 4 shows the changes in resistance of the sensor with temperature in different atmospheres. As indicated in this figure, both curves in dry and wet air fit straight lines quite well. The resistance in wet air is only slightly lower than that in dry air. Thus, in an atmosphere of air, humidity only has a minor influence on the sensor resistance in this considered temperature range. But, this effect becomes stronger when the measurements were performed in 1%O_2 gas (the remainder being N_2). Finally, measurements were performed in dry and wet N_2 gas. Here, an even greater influence of water vapor on the sensor resistance is observed. Generally, the three lines corresponding to the dry conditions of different P_{O_2} appear parallel and the effect of water vapor on the resistance/temperature behavior of the sensor is more pronounced at lower oxygen partial pressures.

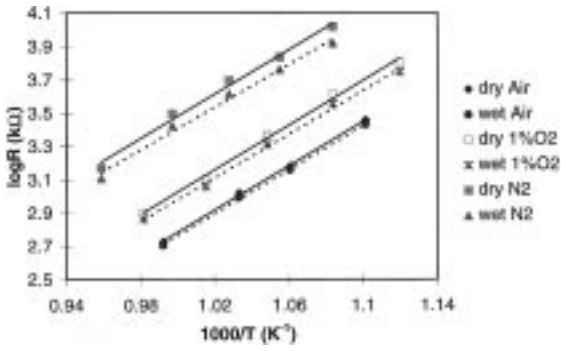

Fig. 4. Plots of $\log R$ versus $1000/T$ for the sensor in different dry and wet conditions.

4.2. Response to Oxygen Partial Pressure Changes in the Presence of Water Vapor

The cross sensitivity of the sensor to P_{O_2} and P_{H_2O} was evaluated at 700°C by varying the oxygen partial pressure from air (0.21 bar) to N_2 $(2.5 \times 10^{-5}\,\text{bar})$ and the water content of the carrier gas from 5 to 95% *RH*, respectively. Figure 5 shows a double logarithmic diagram of the resistance of the sensor as a function of oxygen partial pressure. It turns out that all the curves $(\log R$ vs. $\log P_{O_2})$ appear linear in the considered oxygen partial pressure range and that the resistance increases monotonically with decreasing oxygen partial pressure. However, by increasing the water content of the carrier gas, the slope $(-1/m)$ of the curves $(\log R \propto \log P_{O_2})$ diminishes. Correspondingly, the value of m increases from 4.34 through 4.55 to 4.76 with increasing relative humidity from 5% through 40% to 95% *RH*.

4.3. Resistance of the Sensor as a Function of Relative Humidity at Constant Oxygen Partial Pressure and Temperature

Figure 6 shows the response of the sensor to different relative humidities at 710°C in 1% O_2/N_2 gas. It can be seen that the resistance of the sensor decreases monotonically with increasing water content in the carrier gas. The total relative resistance change

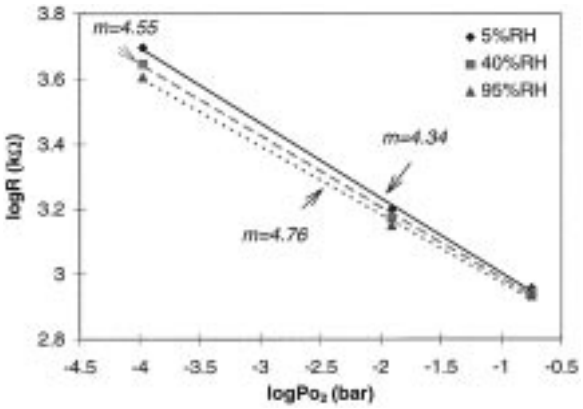

Fig. 5. $\log R$ versus $\log P_{O_2}$ of the Mg-doped $SrTiO_3$ sensor at 700°C.

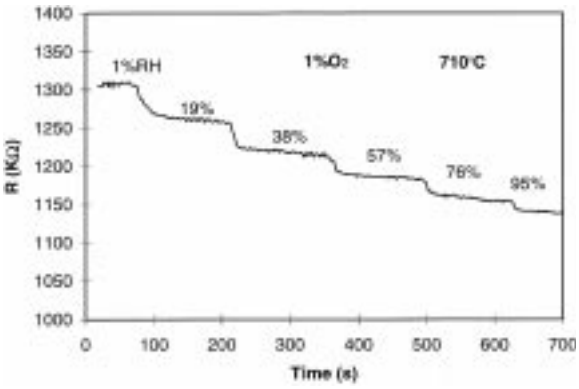

Fig. 6. Resistance of the sensor at 710°C in gases with different humidities.

$(\Delta R/R_d)$ is about 12%, where R_d represents the resistance value in a dry $(1\%\ RH)$ atmosphere of 1% O_2/N_2 gas.

4.4. *Resistance of the Sensor with Respect to Relative Humidity and Oxygen Partial Pressure*

This experiment was performed in the P_{O_2} range from 2.5×10^{-5} to 0.21 bar and the humidity range from 5% to 95% *RH*. Figure 7 shows the normalized resistance *S* (the resistance value at any given humidity with respect to the resistance at $RH = 5\%$) of the sensor versus relative humidity measured in different oxygen partial pressure conditions. As shown in this figure, *S* decreases with increasing relative humidity and this trend is similar in the different P_{O_2} atmospheres. However, the strongest effect of water vapor is, in fact, found at the lowest oxygen partial pressures.

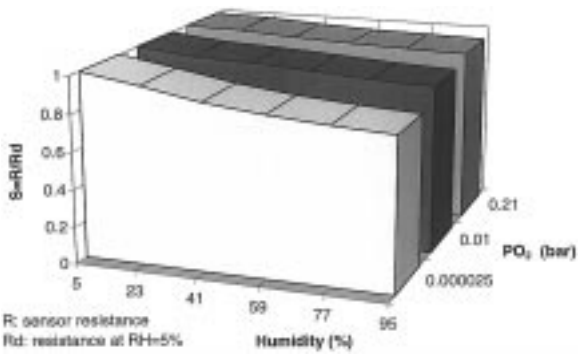

Fig. 7. Normalized resistance *S* with respect to the resistance value at $RH = 5\%$ versus relative humidity of the Mg-doped $SrTiO_3$ sensor at 700°C.

4.5. *Resistance Behavior of the Sensor with Respect to Relative Humidity and Temperature*

Figure 8 shows the normalized resistance *S* of the sensor versus relative humidity as a function of temperature investigated in the 1% O_2/N_2 gas, where *S* again is the normalized resistance value at any given humidity, in this case with respect to the resistance at $RH = 1\%$.

As indicated in this figure, the normalized resistance *S* depends both on relative humidity and temperature. Basically, *S* decreases with increasing water content of the carrier gas in the whole temperature range. It is also worth noting that, the dependence of resistance on relative humidity becomes less significant as the temperature is raised. The maximum water interference on the sensor response is observed at lower temperatures.

5. Discussions

5.1. *Slopes of Plots* $(\log R$ *vs.* $\log P_{O_2})$ *in Different Atmospheres*

The assumption made in this work, that, in the high oxygen partial pressure region $(P_{O_2} > 10^{-6}$ bar), Mg-doped $SrTiO_3$ exhibits *p*-type conduction is confirmed in Fig. 5 as the resistance of the sample is found to decrease with increasing oxygen partial pressure in the considered oxygen partial pressure region. In Fig. 5, the slopes $(-1/m)$ in the observed P_{O_2} range vary between $-1/4$ to $-1/5$ and the value of $1/m = 1/4.35$ is achieved in the approximate dry

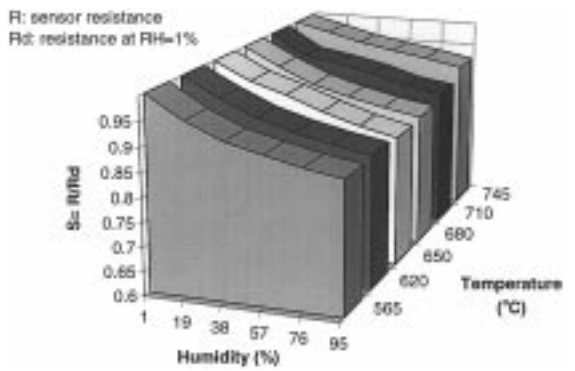

Fig. 8. Normalized resistance *S* with respect to the resistance value at $RH = 1\%$ versus relative humidity of the Mg-doped $SrTiO_3$ sensor in 1% O_2/N_2.

condition (5% *RH*). This value is comparatively smaller than the theoretical value $(1/m = 1/4)$. However, this is commonly observed in polycrystalline materials [15] and is even closer to 1/4 compared to the value ($m = 0.22$ equal to $1/m = 1/4.55$) measured by J. Gerblinger et al. [16] for undoped $SrTiO_3$. It is also clear in Fig. 5 that, the slope $(-1/m)$ is diminished by increasing the humidity in accordance with Eq. (21), which expresses the influence of the water vapor pressure on this slope.

5.2. *Effect of the Dopant*

According to Eq. (2), $m = 4$ is derived for Mg-doped $SrTiO_3$. In a comparison with the literature on strontium titanate [17], $m = 4$ is also expected for undoped $SrTiO_3$ material in the *p*-type region due to the presence of minor acceptor impurities. However, in the present work, owing to the addition of the acceptor MgO into $SrTiO_3$, a high concentration of oxygen vacancies is generated, which enhances the uptake of oxygen into the lattice according to Eq. (1). Therefore the *p*-type conduction is enhanced in Mg-doped $SrTiO_3$ and the *p-n* transition is therefore also shifted down to lower oxygen partial pressures in this oxide [18].

5.3. *Resistance as a Function of Water Vapor Pressure at Constant Temperature and* P_{O_2}

According to Eq. (20), the inverse total resistance is proportional to $P_{H_2O}^{1/2}$ at a fixed given P_{O_2} if the temperature is kept constant. This illustrates that the resistance of the sensors should be expected to decrease with increasing partial pressure of the water vapor and this tendency is indeed observed in Fig. 6. In accordance with Eq. (20), replotting the data of Fig. 6 in terms of the reciprocal of resistance $(1/R)$ as a function of $P_{H_2O}^{1/2}$ gives, in fact, straight lines as shown in Fig. 9, which further supports the validity of the assumptions made in the theoretical considerations.

5.4. *Thermal Activation Energy for Hole Conduction*

From the slopes of the curves corresponding to the dry conditions in Fig. 4, the thermal activation energy for hole conduction was calculated according to Eq. (8) to be:

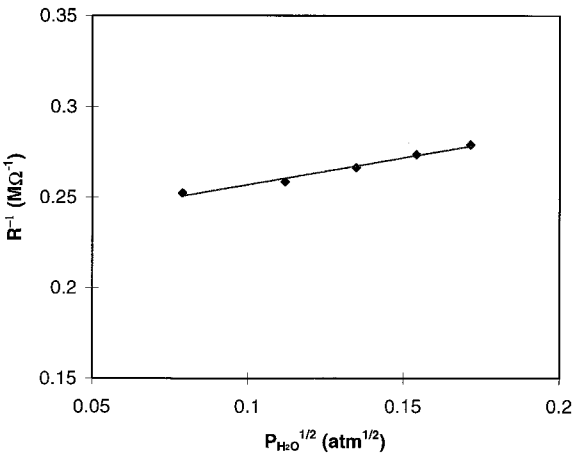

Fig. 9. Plot of reciprocal resistance of the sensor against $P_{H_2O}^{1/2}$ at 710°C in 1% O_2 atmosphere.

$$E_p = 1.319 \pm 0.001\ \text{eV} \tag{28}$$

This value is in fairly good agreement with the value of 1.35 eV quoted for undoped $SrTiO_3$ in the literature [19], but is somewhat smaller than the value of 1.59 eV for undoped $SrTiO_3$ in another reference [20].

5.5. *Thermal Activation Energy for Proton Conduction*

Replotting the data of Fig. 4 in the form of $\log(1/R_2 - 1/R_1)$ vs. $1000/T$ in accordance with Eq. (26), straight lines are indeed observed as shown in Fig. 10. Thus, from the slope of these curves, the thermal activation energy for proton conduction can be calculated to be:

$$E_{H_i^\bullet} = 1.246 \pm 0.002\ \text{eV} \tag{29}$$

No relevant data for $SrTiO_3$ so far can be quoted to make a similar comparison. However, compared to the value of 0.64 eV for $BaCeO_3$ [21], the value of 1.246 eV for $SrTiO_3$ is much higher.

5.6. *Normalized Resistance* S *with Respect to Water Partial Pressure*

In Fig. 7, *Rd* is defined as the resistance value at $RH = 5\%(P_{H_2O} = 1.6 \times 10^{-3}\ \text{atm})$.

If applying Eq. (20) for this atmosphere, the normalized resistance *S* can be expressed as:

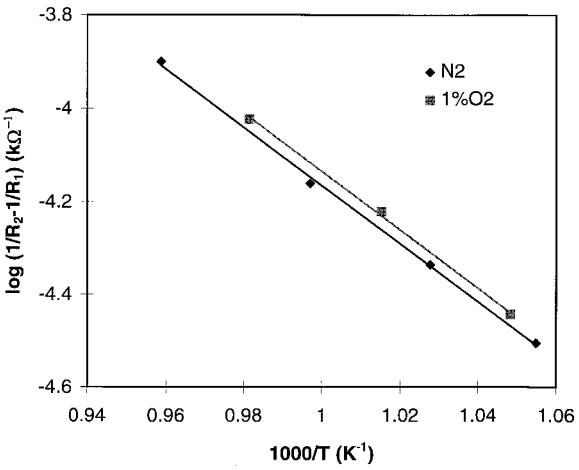

Fig. 10. Plots of $\log(1/R_2 - 1/R_1)$ vs. $1000/T$ for the Mg-doped $SrTiO_3$ sensor.

$$S = R/R_d = \sigma_d/\sigma = (\sigma_p^O P_{O_2}^{1/4} + \sqrt{1.6\times10^{-3}}\sigma_{H_i^\bullet}^O) \Big/ (\sigma_p^O P_{O_2}^{1/4} + \sigma_{H_i^\bullet}^O P_{H_2O}^{1/2}) = (\sigma_p^O P_{O_2}^{1/4} + 0.04\sigma_{H_i^\bullet}^O)/(\sigma_p^O P_{O_2}^{1/4} + \sigma_{H_i^\bullet}^O P_{H_2O}^{1/2}) = 1 - \sigma_{H_i^\bullet}^O (P_{H_2O}^{1/2} - 0.04)/(\sigma_p^O P_{O_2}^{1/4} + \sigma_{H_i^\bullet}^O P_{H_2O}^{1/2}) \quad (30)$$

Differentiating this equation with respect to P_{H_2O}, the following expression can be derived:

$$\frac{dS}{dP_{H_2O}} = -\frac{1}{2}(\sigma_p^O P_{O_2}^{1/4} + 0.04\sigma_{H_i^\bullet}^O)\sigma_{H_i^\bullet}^O P_{H_2O}^{1/2} \Big/ (\sigma_p^O P_{O_2}^{1/4} + \sigma_{H_i^\bullet}^O P_{H_2O}^{1/2})^2 \le 0 \quad (31)$$

which indicates that the value S decreases monotonically with increasing water vapor pressures as confirmed by the results shown both in Figs. 7 and 8.

5.7. *Normalized Resistance* S *with Respect to Oxygen Partial Pressure*

Differentiating Eq. (30) with respect to P_{O_2} gives:

$$\frac{dS}{dP_{O_2}} = \frac{1}{4}(P_{H_2O}^{1/2} - 0.04)\sigma_{H_i^\bullet}^O \sigma_p^O P_{O_2}^{-3/4} \Big/ (\sigma_p^O P_{O_2}^{1/4} + \sigma_{H_i^\bullet}^O P_{H_2O}^{1/2})^2 \ge 0 \quad (32)$$

which reveals that the normalized resistance S decreases monotonically with decreasing oxygen partial pressures as illustrated in Fig. 7. As the deviation of S from 1 represents the degree of water influence on the sensor resistance, it also implies that a stronger influence of water vapor on the sensor resistance should be expected at lower oxygen partial pressures.

5.8. *Proton Transport Number*

Furthermore, it can also be observed in Fig. 8 that, the effect of water on the normalized resistance S is somewhat more marked at lower temperatures. This can be explained from Eq. (27), which gives the transport number for Mg-doped $SrTiO_3$.

In the case of constant P_{O_2} at 0.01 bar, Eq. (27) can be written as:

$$t_{H_i^\bullet} = 1\Big/\left\{1 + \frac{A_1}{A_2}\sqrt[4]{0.01}P_{H_2O}^{-1/2}\exp(E_{H_i^\bullet} - E_p)/kT\right\}$$

which by using the values of $E_{H_i^\bullet}$ (1.246 eV) and E_p (1.319 eV) gives:

$$t_{H_i^\bullet} = 1\Big/\left\{1 + 0.3162\frac{A_1}{A_2}P_{H_2O}^{1/2}\exp(-0.073/kT)\right\} \quad (33)$$

From Eq. (33), it can be determined that $t_{H_i^\bullet}$ decreases with increasing temperature, suggesting that the proton transport number tends to be reduced at high temperatures, which also indicates that the hole conductivity becomes more dominating at higher temperatures. This can easily explain why the presence of water has less effect on the resistance of the sensor at higher temperatures.

6. Conclusions

This investigation shows that Mg-doped $SrTiO_3$ sensors exhibit pure p-type conduction in an atmosphere free from water. However, in an atmosphere containing water vapor, a reducing effect of the water vapor on the resistance of the sensors is observed. The resistance of the sensors decreases monotonically with increasing water content in the carrier gas. The extent of this effect depends both on temperature and oxygen partial pressure, with the maximum effect at lower temperatures as well as at lower oxygen partial pressures. A model based on defect chemistry and conduction mechanisms is proposed. It is assumed that water can be dissolved in Mg-doped $SrTiO_3$ by the formation of protonic species and therefore a

partial protonic conduction contributes to the total conduction in humid atmospheres. This model satisfactorily explains the experimental results and based on this model, the thermal activation energies for hole and proton conduction are also obtained. The measurements furthermore indicate that the electronic hole conduction still plays a dominating role within the total conduction even in humid atmosphere. In the presence of water vapor, the resistance of these sensors still depend on oxygen partial pressure according to the standard expression and these sensors can therefore still be used as oxygen sensors in humid atmospheres.

References

1. Jianzhong Zhu and Congxin Ren, *Sensors and Actuators B*, **32**, 209 (1996).
2. H. Meixner, J. Gerblinger, and M. Fleischer, *Sensors and Actuators B*, **15–16**, 46 (1993).
3. Chunying Yu, Y. Shimizu, and H. Arai, *J. Mat. Sci. Let.*, **8**, 765–766 (1989).
4. Xiaohua Zhou, O. Toft Sørensen, and Yulong Xu, *Sensors and Actuators B*, **41**, 177 (1997).
5. J. Gerblinger, U. Lampe, and H. Meixner, *Sensors and Actuators B*, **18–19**, 530 (1994).
6. C. Cantalini, M. Faccio, G. Ferri, and M. Pelino, *Sensors and Actuators B*, **18–19**, 437 (1994).
7. Chunying Yu, Y. Shimizu, and H. Arai, *Sensors and Actuators B*, **14**, 317 (1988).
8. Xiaohua Zhou, O. Toft Sørensen, and Yulong Xu, *Sensors and Actuators B*, **41**, 180 (1997).
9. R. Moos and K.H. Härdtl, *J. Am. Ceram. Soc.*, **80**(10), 2549 (1997).
10. D.P. Sutija, T. Norby, and P. Björnbom, *Solid State Ionics*, **77**, 167 (1995).
11. N. Bonanos, K.S. Knight, and B. Ellis, *Solid State Ionics*, **79**, 163 (1995).
12. A.S. Nowick and Yang Du, *Solid State Ionics*, **77**, 137–141 (1995).
13. H. Uchida, N. Maeda, and H. Iwahara, *Solid State Ionics*, **11**, 120 (1983).
14. T. Norby, *Advances in ceramics*, **23**, 107–123 (1987).
15. N.H. Chan, R.K. Sharma, and D.M. Smyth, *J. Electrochem. Soc.*, **128**(8), 1762 (1981).
16. J. Gerblinger, M. Hausner, and H. Meixner, *J. Am. Ceram. Soc.*, **78**(6), 1453 (1995).
17. U. Balachandran and N.G. Eror, *J. Solid State Chem.*, **39**, 358 (1981).
18. N.G. Eror and U. Balachandran, *J. Am. Ceram. Soc.*, **65**(9), 430 (1982).
19. U. Balachandran and N.G. Eror, *J. Solid State Chem.*, **39**, 357 (1981).
20. J. Gerblinger, H. Gabler, R. Mock, and H. Meixner, *Sensors and Actuators B*, **15–16**, 397 (1993).
21. W. Munch, G. Seifert, K.D. Kreuer, and J. Maier, *Solid State Ionics*, **97**, 39–44 (1997).